Journal of Applied Polymer Science

Improvement of mechanical properties of polylactic acid adhesion joints with bio-based adhesives by using air atmospheric plasma treatment

Amparo Jordá-Vilaplana,[1] Lourdes Sánchez-Nácher,[2] Vicent Fombuena,[2] Daniel García-García,[2] Alfredo Carbonell-Verdú[2]

[1]Departamento de Ingeniería Gráfica (DIG), Universitat Politècnica de València (UPV), 03801 Alcoy, Spain
[2]Instituto de Tecnología de Materiales (ITM), Universitat Politècnica de València (UPV), 03801 Alcoy, Spain
Correspondence to: A. Jordá-Vilaplana (E-mail: amjorvi@upv.es)

ABSTRACT: The packaging industry generates a high volume of wastes; so that, there is a high demand of biodegradable materials, which do not damage the environment. Nowadays, there is an interesting consumption of polylactic acid (PLA) due to its biodegradable features. This work focuses on the improvement of mechanical properties of PLA adhesion joints for uses in the packaging industry. In order to achieve that purpose, atmospheric plasma treatment is used to selectively modify PLA surface properties. The obtained experimental results show that the atmospheric plasma treatment is suitable to increase the mechanical performance of PLA–PLA adhesive joints. Optimum conditions for the atmospheric plasma treatment were obtained with a nozzle–substrate distance of 10 mm and an advance rate in the 100–300 mm s^{-1} range; for these particular conditions, the effectiveness of the surface modification is the highest. The main plasma-acting mechanisms are microetching together with the insertion of polar groups which lead to an interesting synergy that causes a remarkable increase in mechanical properties of adhesion joints. In particular, the shear strength of untreated PLA–PLA adhesion joints is close to 50 N cm^{-2} and this value is increased up to values of about 168.7 N cm^{-2} with optimum plasma treatment conditions. This indicates that atmospheric plasma treatment is both a technical and an environmental friendly technique to improve mechanical performance of PLA adhesive joints. © 2015 Wiley Periodicals, Inc. J. Appl. Polym. Sci. **2015**, *132*, 42391.

KEYWORDS: adhesives; biodegradable; mechanical properties

Received 2 February 2015; accepted 21 April 2015
DOI: 10.1002/app.42391

INTRODUCTION

Nowadays, the environmental concerns and sustainability in materials engineering are acquiring special relevance. This situation has produced an interesting increase in research on new materials and different topics such as environmentally friendly, biodegradable, ecological, bio-based, compostable, and so on are being considered. For this reason, polymeric materials from natural sources are occupying important research lines with the aim of substituting petroleum-based polymers. Packaging industry is one of the main fields of waste production.[1] The packaging industry for food products demands design flexibility in the material, low density, and low cost; therefore, the use of polymers is very widespread. Polylactic acid (PLA)[2] is a biodegradable polymer from natural sources that has similar properties to polyolefins,[3] which have been traditionally used in the packaging industry.[4] PLA comes from the lactic acid produced by the anaerobic fermentation of substrates that have carbon, as for example glucose, lactose, etc. Nowadays, it is already used in the food industry, representing the 85% consumption of the total production of this polymer. It is possible to find it in thermoformed packages: cups, containers, bottles, films, textile fibers, bags or teabags, single-use crockery items, etc.[5–7]

From the point of view of the container design, the formation of adhesive joints is sometimes required. Due to the inherently low wettability that most of polymers have, PLA is characterized by relatively low surface energy which leads to poor adhesive properties; therefore, hydrophilicity must be increased using surface modification techniques.

Surface modification treatments of polymers based on atmospheric plasma technologies are acquiring high relevance at industrial level. In fact, these treatments show an easy implementation in manufacturing processes, easy automation; in addition, atmospheric plasma techniques are environmentally friendly, as it does not generate wastes.[8–10] Atmospheric plasma allows selective modification of the topmost layers without affecting the bulk material. Previous studies have been carried out with PLA and atmospheric plasma focusing on improving

energy surface for a better adhesion to substrates PLA–PLA.[11,12] By the control of the process parameters, nozzle–polymeric substrate distance and substrate advance rate, different surface properties can be tailored, as for example the wettability of inks and dyes, adhesion,[13–15] growth of other layers, etc. In general, an interesting increase of the solid surface energy is produced by the action of two main plasma-acting mechanisms. From the physical point of view, atmospheric plasma produces surface abrasion that brings a change in the surface roughness. From the chemical point of view, the highly energetic species in the air plasma react with the topmost layers of the polymer surface and the overall effects are chain scission, hydrogen removal (and subsequent free radical formation), and surface oxidation.[16,17] These mechanisms have a synergistic effect that produces an important increase in polymer surface energy; therefore, it also improves its hydrophilic behavior.[18,19]

In this research work, atmospheric air plasma treatment is used on PLA surface in order to improve mechanical performance of PLA–PLA adhesion joints with the main aim of increasing the relatively low PLA surface energy. The adhesive used are ecologic bio-based. Adhesives used are from its most natural resources (55%), these stickers have the advantage of being biodegradables, as well as the substrate used.[20]

In order to achieve it, the optimal conditions (plasma processing parameters) are determined. Changes in surface topography were evaluated by using scanning electron microscopy (SEM) and atomic force microscopy (AFM) techniques; in addition, chemical changes at the topmost layers were followed by using X-ray photoelectron spectroscopy (XPS).[21]

EXPERIMENTAL

Materials

PLA commercial grade PLA 6201D was supplied in pellet form by Nature Works LLC (Nature Works LLC, Minnetonka, Minnesota, USA). This material was injection molded in rectangular sheets sizing 160 × 60 × 2.2 mm^3 in an industrial injection molding machine Mateu & Sole mod. 270/5 (Mateu & Sole, Barcelona, Spain). The injection parameters used were as follows: injection temperature 170°C, mold temperature 25°C, injection speed 40 ms^{-1}, pack/hold 800 bar, and pack/hold time 9 ms^{-1}.

A commercial adhesive grade EcoPoxy Fast Hardener supplied by Ecopoxy Systems Company (Providence, EEUU) was used to form PLA–PLA adhesion joints. Ecopoxy is a partially bio-based adhesive with epoxidized soybean oil and it finds typical applications as adhesive or pultrusion with fibers. The physical data is boiling point: >150°C, 300°F, the vapor pressure at 76 mmHg to 20°C, 68°F, the vapor density is 3.56, 48.8°C Vicat temperature and Shore D hardness 68, is moderately soluble in water, the appearance is pale straw colored liquid and moderate amine odor. It is suitable for bonding different materials such as wood, fiberglass, metal, glass, and ceramics.[20]

Sample Preparation

Air atmospheric plasma was generated with a "Plasma Jet RD 1004" reactor supplied by Plasmatreat (Plasmatreat GmbH, Steinhagen, Germany). It consists on a plasma generator, which works at 50/60 Hz, 230 V, and 16 A, with a discharge frequency of 17 kHz and a discharge voltage of 20 kV. Pressurized (2 bar) dried air was used for plasma generation. Different nozzle–substrate distances between 10 and 20 mm and several sample advance rates ranging from 100 and 1000 mm s^{-1} were used. The advance rate is the speed of the movement of the polymer situated in a slicer guide.

Table I. Contact Liquids with Its Surface Energy Values and Their Polar and Dispersive Components

Test liquid	Water	Glycerol	Diiodomethane	Formamide
γ_s^d(mJ m^{-2})	22.0	34.0	48.5	32.3
γ_s^p(mJ m^{-2})	50.2	30.0	2.3	26.0
γ_s (mJ m^{-2})	72.2	64.0	26.0	58.3

Characterization Techniques

Surface Wettability. Contact angle measurements were examined with an Easydrop Standard KRÜSS goniometer model FM140 (KRÜSS GmbH, Hamburg, Germany). This model has a precision of ±0.1° and a measurement range between 1 and 180°. In order to determine the contact angle, the DROP SHAPE ANALYSIS SW21 (DSA1) software supplied by the provider was used. This process was done with four different test liquids with different polarities in order to estimate the surface energies.

Four different test liquids were used for contact angle measurements and subsequent surface energy calculations: stabilized diiodomethane (99% of purity) supplied by Acros Organics (Acros Organics, Geel, Belgium), double-distilled water, formamide, and glycerol 99%, extra pure for analysis (reagent grade) ACS from Scharlau Chemie S.A. (Scharlab S.L. Barcelona, Spain). Table I summarizes the surface free energies (γ_s) of the different liquids with their corresponding polar (γ_s^p) and dispersive (γ_s^d) contributions.

In this study, the Owens–Wendt method was used; this estimates the solid surface free energy of each sample, this method allows determining the polar and dispersive contributions of the components.

$$\gamma_l \cdot (1 + \cos(\theta)) = 2(\gamma_s^d \cdot \gamma_l^d)^{1/2} + 2(\gamma_s^p \cdot \gamma_l^p)^{1/2} \quad (1)$$

In this equation, "θ" is the contact angle, "γ_l" is the surface tension of the liquid, and "γ_s" is the surface tension of the solid or surface free energy. The terms with the superscripts "d" and "p" are the dispersive and polar component of surface free energy. The Owens–Went equation is an equation of the type "$y = a + bx$" which can be represented $(\gamma_l^p)^{1/2}/(\gamma_l^d)^{1/2}$ versus $\gamma_l \cdot (1 + \cos(\theta))/2(\gamma_l^d)^{1/2}$. The slope of the line obtained will be $(\gamma_s^p)^{1/2}$ while the axis point "Y" straight cut that will $(\gamma_s^d)^{1/2}$. The total surface free energy is the sum of these two components.[22–27]

Atomic Force Microscopy. AFM was used in order to evaluate changes in surface roughness and topography of PLA as a consequence of the air plasma treatment. This analysis was made with a Multimode AFM equipment, equipped with a nanoscope ADCS controller (Veeco Metrology Group, Cambridge, United

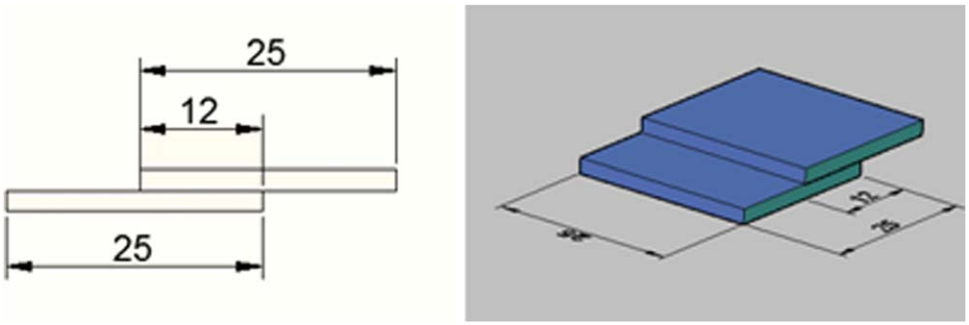

Figure 1. Views of the placement of samples 2d and simulated 3D samples. [Color figure can be viewed in the online issue, which is available at wileyonlinelibrary.com.]

Kingdom), and a silicon cantilever (Nano World Point probe ® NCH) with a constant force of 42 N m^{-1} and a resonance frequency of 320 kHz. The root-mean-squared roughness (R_{rms}) values for each plasma condition were determined from collected images of 20 × 20 μm^2 in size.

X-ray Photoelectron Spectroscopy (XPS). Chemical changes at the topmost layers of PLA (untreated and plasma-treated) were obtained by using X-ray photoelectron spectroscopy (XPS) in a V6-Microtech Multilab (V6 Microtech Ltd, UK) with a pass energy of 50 eV and a radiation of MgKα (1253.6 eV) anodic with constant mode of energetic analysis and a pressure of 5 × 10^{-10} mbar. The *C* (1s) was set to 284.6 eV. Binding energies (with accuracy of ±0.2 eV) were obtained with the Peak-fit software provided with the spectrometer XPS.[28]

Mechanical Properties of PLA–PLA Adhesion Joints. PLA–PLA adhesion joints were tested in shear mode following the ISO 13445 standard. The shear tests were carried out in a universal test machine IBERTEST ELIB 30 (S.A.E. Ibertest, Madrid, Spain). Squared PLA samples 25 × 25 × 2 mm^3 were used to prepare adhesion joints. The adhesion varied between 10 and 12 mm Figure 1. The selected cross-head speed for the test was 50 mm min^{-1} (Figure 1). At least five samples were tested for each plasma condition.

Scanning Electron Microscopy. In order to observe the morphology of the fractured surface from shear test of PLA–PLA adhesion joints, an SEM model PHENOM (FEI Company, Oregon, USA) working at an electron acceleration of 5 kV was used. Samples were previously subjected to a sputter coating process with a gold–palladium alloy in a Sputter Coater EMITECH mod. SC7620 (Quorum Tech. Ltd., UK).

RESULTS AND DISCUSSION

Wettability Variation of the Polylactic Acid (PLA) Substrate Surface

Figure 2 shows the variation of the contact angle decrease ($\Delta\theta = \theta_{untreated} - \theta_{treated}$) depending on the advance rate of the sample, for four PLA–nozzle distances: 6, 10, 14, and 20 mm. For low distances and low advance rates, the decrease in the contact angle value is high. The smaller contact angles were obtained in the PLA surfaces treated with air atmospheric plasma (comparing them with the untreated surface) showing an important increase in surface wettability. Optimum results were obtained with advance rates (100–300 mm s^{-1}) and nozzle–substrate distance (around 10 mm); under these conditions, the surface modification treatment was more effective. Lower distances lead to surface degradation of the samples due to oxidative plasma power; therefore, the surface modification achieved was not as efficient. For higher nozzle–PLA substrate distance, the contact angle reduction ($\Delta\theta$) was lower since the plasma species were highly unstable and the effects of them were lost for high distances. For a distance of 20 mm, $\Delta\theta$ did not show a so-marked decrease because of the advance rate increase.

Figure 3 shows the variation of the surface free energies in terms of the PLA advance rate for different nozzle–sample distances. It is important to remark the increase in surface free energy from values close to 37.1 mJ m^{-2} for the untreated PLA, up to maximum values of about 60 mJ m^{-2} for a plasma-treated PLA sample with a nozzle–sample distance of 10 mm and an advance rate of 100 mm s^{-1}. The air atmospheric plasma treatment increased considerably the surface free energy of the PLA substrate. The best results were obtained for a nozzle–substrate distance of 10 mm and advance rates between 100 and 500 mm s^{-1}, and nozzle–substrate distance of 6 mm and advance rates ranging from 300 to 400 mm s^{-1} both conditions with surface free energy values higher than 50 mJ m^{-2}. However, when a distance of treatment is 6 mm, a degradation in the surface of the polymer is obtained, due to a too aggressive treatment. For this reason, the optimal distance is concluded, that is 10 mm.

Surface Topography Variations

The analysis of the untreated PLA surface by atomic force microscopy (AFM) gives an average roughness value of 12.1 nm. The air atmospheric plasma microetching over the polymeric surface was quantified with a clear increase in the surface microroughness; we can observe its values in Table II.

The high average roughness value corresponds to a nozzle–substrate distance of 6 mm and an advance rate of 100 mm s^{-1}, being this average roughness (R_{rms}) of 120.5 nm. If we compared it with the untreated PLA surface, this roughness is 10 times higher. At highest roughness, the total surface area

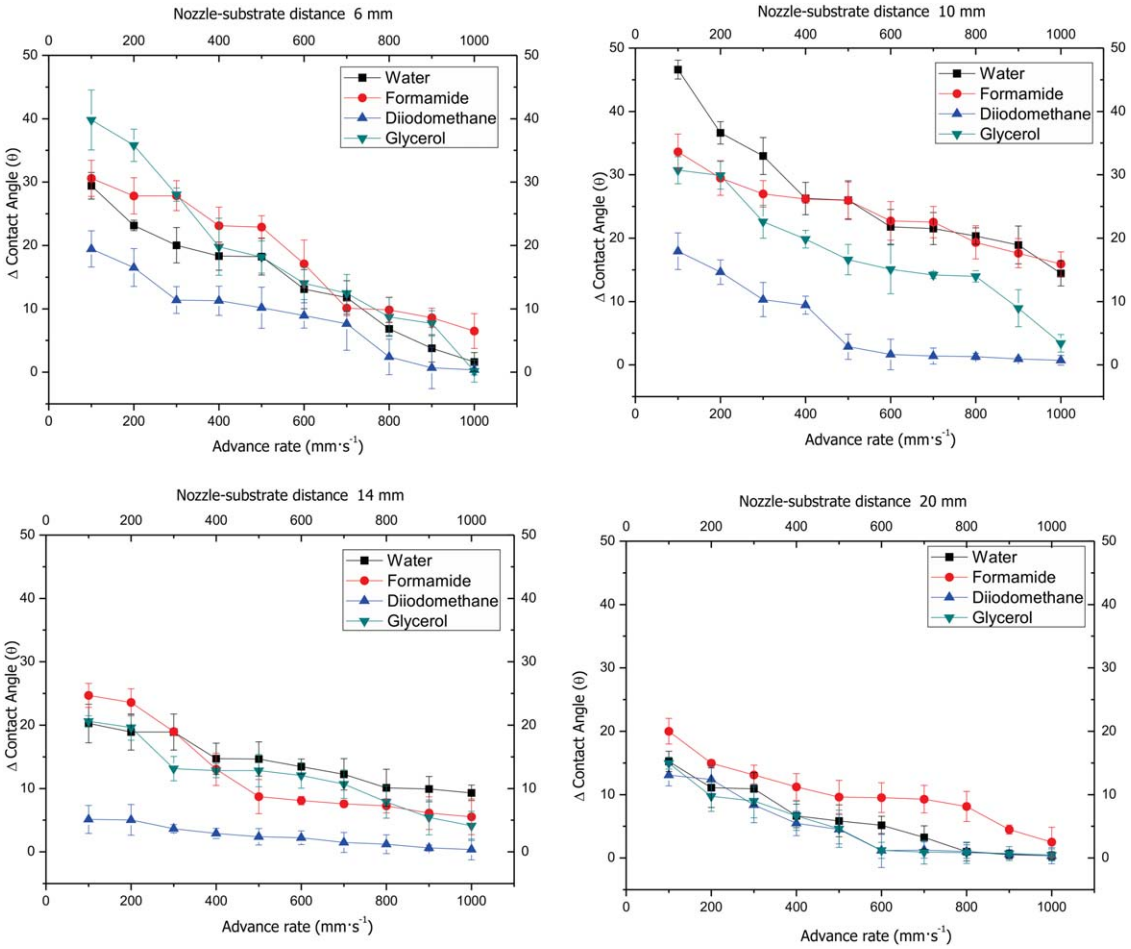

Figure 2. Variation of the contact angle change ($\Delta\theta = \theta_{untreated} - \theta_{treated}$) at different advance rates and at different nozzle–substrate distances (6, 10, 14, and 20 mm) for the four test liquids. [Color figure can be viewed in the online issue, which is available at wileyonlinelibrary.com.]

increased and, subsequently, adhesion properties were enhanced. For these particular conditions, the atmospheric plasma treatment was very aggressive; therefore, material removal increases. This aggressiveness decreased when the advance rate and/or nozzle–substrate distance increase, producing less abrasion and a decrease in the roughness values, as we can observe in Table II. According to Table II, the best results were AFM substrate to a nozzle distance of 6 mm and advance rate of 100 mm s^{-1} but not optimum for the study in general because final conclusions indicate that optimal treatment conditions were 10 mm nozzle–substrate distance and advance rate of 100–300 mm s^{-1} because they did not cause degradation of the sample.

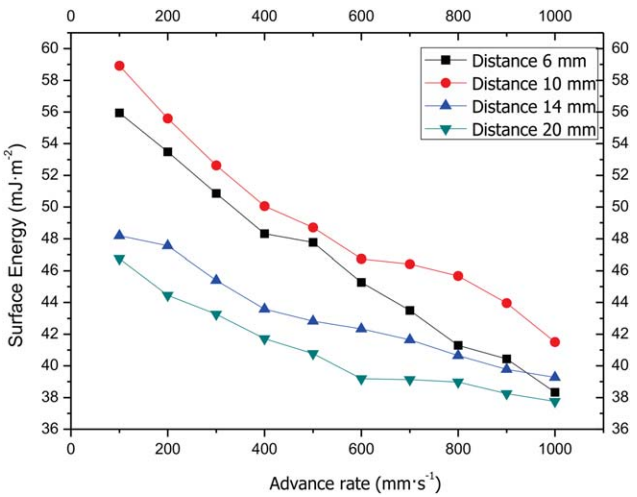

Figure 3. Variation of the surface free energy (γ_S) of PLA surface vs advanced rate taking into consideration different nozzle–substrate distances (6, 10, 14, and 20 mm) in the atmospheric plasma reactor. [Color figure can be viewed in the online issue, which is available at wileyonlinelibrary.com.]

Table II. Average Roughness Values (R_{rms}) of the PLA Samples Treated with Air Atmospheric Plasma at Different Nozzle–Substrate Distances and Different Advance Rates

Average roughness, R_{rms} (nm)				
	Advance rate (mm s^{-1})			
Nozzle–substrate distance (mm)	100	300	700	1000
6	120.5	38.3	38.2	22.5
10	56.9	23.4	21.4	21.3
14	33.6	28.9	26.6	24.9
20	35.6	19.7	14.6	13.8

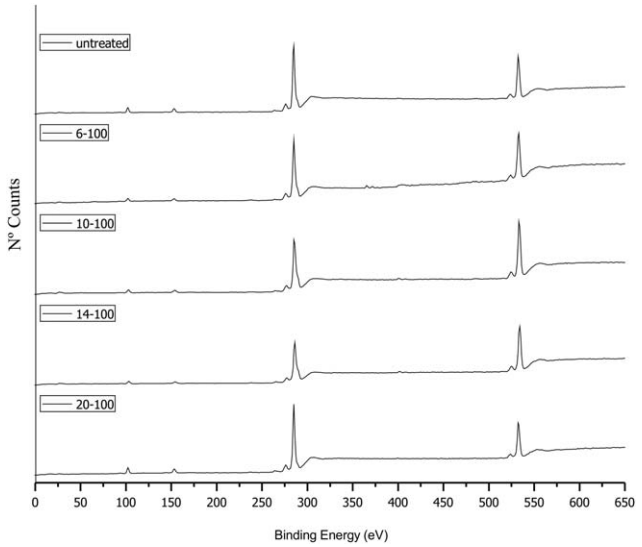

Figure 4. Low-resolution XPS spectra of untreated PLA sheets and plasma-treated (air atmospheric plasma) at different nozzle–substrate distances at a constant advance rate of 100 mm s^{-1}.

Chemical Modifications

Figure 4 shows the low-resolution spectra obtained using XPS for different samples treated at a constant rate of 100 mm s^{-1}. Two significant peaks characterize untreated PLA: the first and more pronounced peak with a binding energy around 285 eV corresponds to the carbon contribution (C 1s) and the second peak, with less intensity, with a binding energy around 533 eV corresponds to oxygen (O 1s). For a nozzle–substrate distance of 6 mm and a low advance rate of 100 mm s^{-1}, comparing it to the untreated material, we can see an increase in the peak belonging to the oxygen contribution (O 1s) transition and a decreased in the peak intensity belonging to transition (C 1s). Moreover, it is possible to see a small peak that corresponds to the nitrogen contribution (N 1s) located at a binding energy around 399 eV that does not appear in the untreated PLA surface. This was because of the air atmospheric plasma effects as many free radicals was formed and these unstable species can react with nitrogen and nitrogen-based species in the plasma gas, thus leading to surface functionalization (mainly species rich in oxygen and in a less proportion, species with nitrogen).[29]

Table III shows the values of the surface atomic composition obtained by the XPS analysis of air atmospheric plasma-treated and untreated PLA samples for a constant advance rate of 100 mm s^{-1} and different nozzle–substrate distances.

The untreated PLA surface is characterized by a carbon atomic percentage of 76.1% and 18.9% of oxygen. The air atmospheric plasma treatment produces a progressive decrease in the carbon percentage when the nozzle–substrate distance increases.

On the contrary, the oxygen percentage increased in a remarkable way, comparing it with the untreated sample for all the analyzed conditions. These results confirmed the PLA chemical functionalization mainly because of the oxygen insertion that comes from the active species in the air plasma (during the plasma action) and reaction of free radicals and unstable species after the plasma treatment and subsequent exposure to oxygen in the air.

Functionalization can be followed by the oxidation level of the PLA surface through the oxygen-to-carbon ratio (O/C ratio). The O/C ratio represents the level of functionalization obtained with the air atmospheric plasma treatment for all the studied conditions. The chemical functionalization of the PLA surface was higher than the untreated PLA surface for all considered conditions. As a consequence of this interaction, the wettability of the surface treated with atmospheric plasma increased. These results showed the increase in the PLA surface polarity due to the effect of the air atmospheric plasma treatment and they were responsible for the improvement of the PLA wettability. The important decrease in the contact angle in the PLA samples treated with air atmospheric plasma and the wettability increase was mainly due to surface activation and roughness change.[30–35]

Effect of Air Atmospheric Plasma on Mechanical Properties of PLA–PLA Adhesion Joints

Figure 5 shows the shear strength of the PLA–PLA adhesion joints with the surface energy values. These two parameters can vary depending on the air atmospheric plasma treatment conditions. Graphically, an important parallelism can be observed between the evolution of the PLA surface free energy and the adhesive joint shear strength. The highest values of shear strength for PLA–PLA adhesion joints corresponded to the highest values of surface energy.

The maximum surface free energy that can be achieved with the plasma treatment is 58.9 mJ m^{-2} for an advance rate of 100 mm s^{-1} and a nozzle–substrate distance of 10 mm. For these particular conditions, the adhesive joint strength was close to 168.7 N cm^{-2}. If it is compared with the shear strength of adhesion joints with untreated PLA surface (50 N cm^{-2}) with a surface energy of 37 mJ m^{-2}, it is possible to triple the strength of the PLA–PLA adhesion joints. For higher nozzle–substrate distances, the atmospheric plasma treatment was less effective. Less abrasion and a less chemical activation of the surface are produced; as a consequence, surface energy is lower. That was to say, less surface wettability was achieved, obtaining lower resistance values of the adhesive joint.

In order to identify the adhesion mechanisms in the substrate–adhesive interface, the morphology of the fractured surfaces

Table III. Variation of the PLA Surface Composition for Untreated Surface and Plasma-Treated (Air Atmospheric Plasma) at a Constant Advance Rate of 100 mm s^{-1} and Different Nozzle–Substrate Distances

		Nozzle–substrate distance (mm)/advance rate (mm s^{-1})			
Atomic composition (%)	Untreated PLA	6/100	10/100	14/100	20/100
C	76.1	74.4	66.6	70.8	69.3
O	18.9	22.3	32.6	27.8	30.3
O/C ratio	0.2	0.3	0.5	0.4	0.4

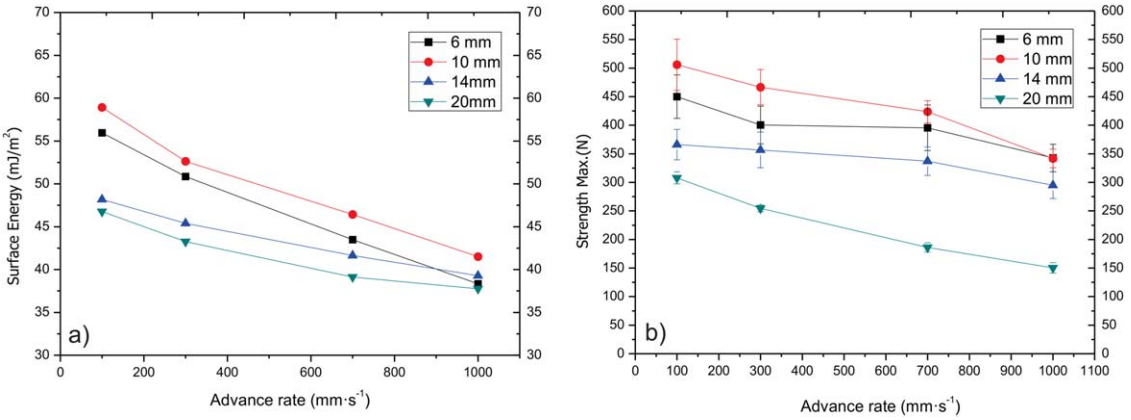

Figure 5. Variation of the surface free energy and the shear strength of PLA–PLA adhesion joints, in terms of the advance rate for different nozzle–substrate distances. [Color figure can be viewed in the online issue, which is available at wileyonlinelibrary.com.]

from shear tests has been obtained by optical microscopy. The visual aspect of the samples was different which was representative for different behavior depending on the plasma-acting conditions. Figure 6 shows the macroscopic images of the fractured surfaces of PLA–PLA adhesion joints from shear tests in terms of the main plasma parameters (nozzle–substrate distance and advance rate).

We can observe two types of morphology in the fractured area where the adhesive was placed. The red square indicates the cohesive failure and the purple square indicates the adhesive failure. There were some areas from the fractured surface completely smooth, without surface roughness, and very uniform, which were characterized by the presence of an adhesive layer on one of the two PLA surfaces of the adhesion joint. This morphology was related to adhesive failure as the adhesive was debonded from the PLA surface. The other type of morphology shows a more irregular aspect, with some roughness and with the formation of little rounded nodules. In this case, there was part of the adhesive in both surfaces of the separated PLA sheets after the shear test and they corresponded to a typical cohesive failure. The areas marked in red

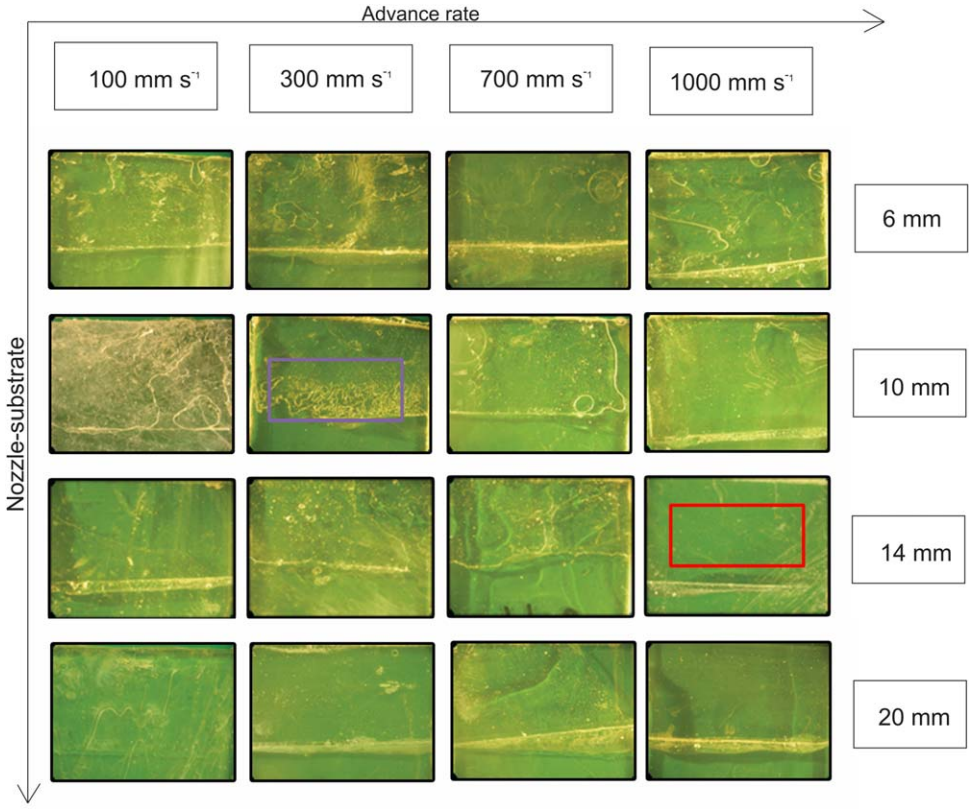

Figure 6. Surface morphology of fractured PLA–PLA adhesion joints by shear tests in terms of the air atmospheric plasma conditions on PLA surface (nozzle–substrate distance and advanced rate). [Color figure can be viewed in the online issue, which is available at wileyonlinelibrary.com.]

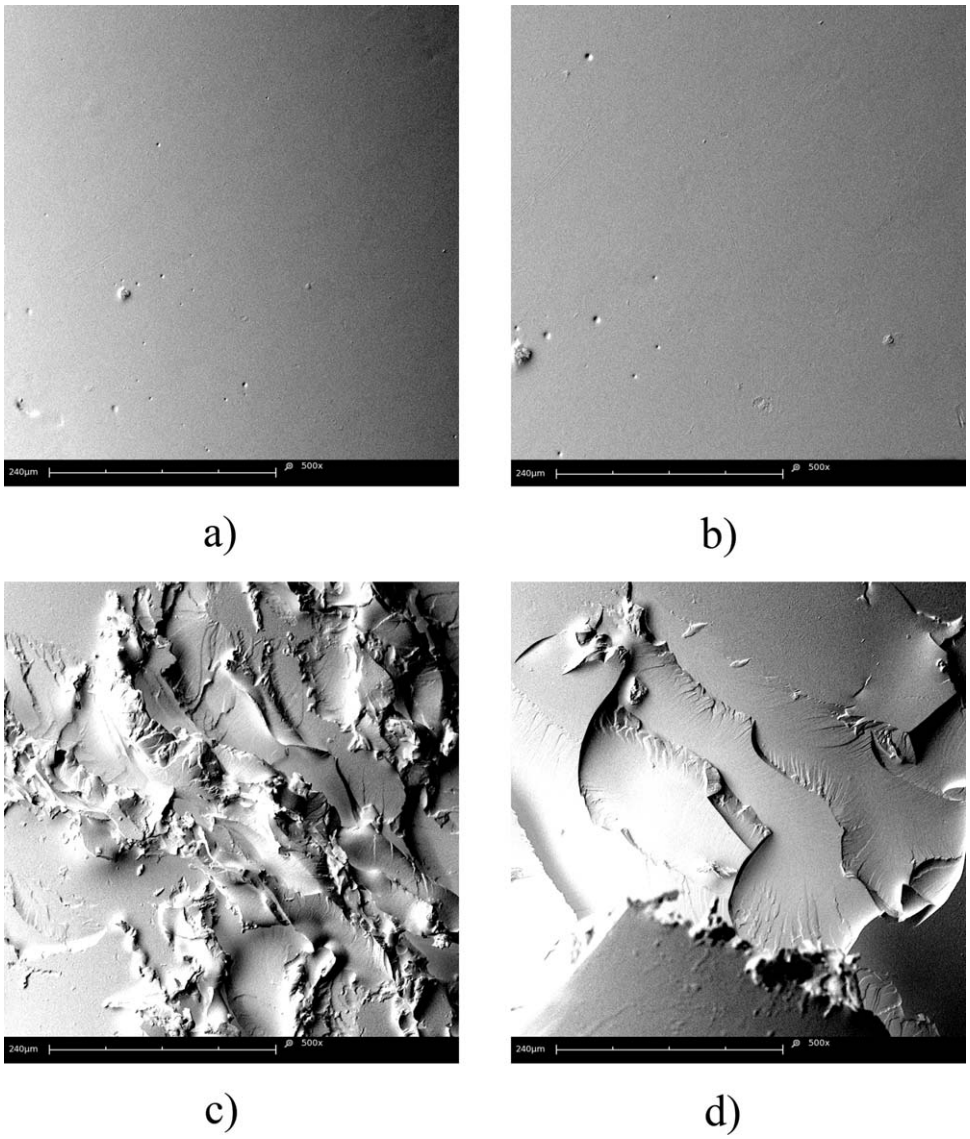

Figure 7. SEM images of fractured surfaces of PLA with smooth and uniform morphology. (a,b) Treated substrate to a nozzle distance of 14 mm and advance rate of 1000 mm s^{-1} and SEM images of fractured surfaces of PLA with roughness morphology (500×). (c,d) Treated substrate to a nozzle distance of 10 mm and advance rate of 300 mm s^{-1}.

and purple will be studied later with SEM as shown in Figures 7 and 8.[36]

The results obtained in the macroscopic analysis of the fractured surfaces after the shear test showed intermediate failure; that was to say, a mix of both types of adhesive failure can be detected: cohesive and adhesive. At low advance rates and/or low distances can be observed little uniform morphology, irregular and with some roughness that corresponds to a good PLA–PLA adhesion. Samples treated with plasma at higher advance rates and/or high distances showed a smooth fractured surface without imperfections fracture surface, this was indicative of poor adhesive properties.[36,37]

Figure 7(a,b) shows the typical SEM micrograph with a smooth and uniform morphology of PLA, due to adhesive failure. This type of morphology can be found for PLA–PLA adhesion joints with untreated PLA surface or with atmospheric plasma treatment with low aggressive conditions (high nozzle–substrate distance and high advance rate).

Figure 7(c,d) shows the abrupt topography of roughness and irregular morphologies of PLA. The surface appearance was highly rough, without uniformity, and with a marked roughness. This dense roughness was produced by the formation of crests and valleys on the adhesive layer. During the shear test, the physical breaking of the adhesive layer was produced; that was to say, a cohesive breaking. We have to take into consideration that this kind of morphology corresponds to shear fracture with high values in the adhesion strength quantified in the previous section.

Both types of morphologies—smooth and rough—were present in most of the fractured surfaces of PLA–PLA adhesion

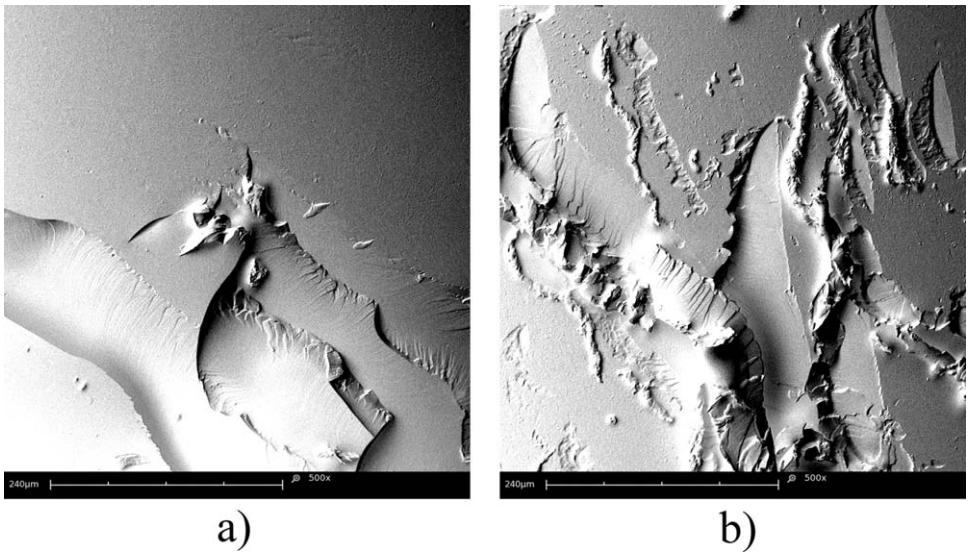

Figure 8. SEM images of fractured surfaces of PLA with mix morphology at 500× treated substrate to a nozzle distance of 14 mm and advance rate of 300 mm s^{-1}.

joints. Figure 8 shows the typical morphologies with both types of surface formations: smooth areas that show low adhesion and rough zones that indicate the surface adhesion improvement.

CONCLUSIONS

The best adhesion properties were obtained with atmospheric plasma process conditions of low advance rate and/or low distances. The highest adhesion values were achieved for a nozzle–substrate distance of 10 mm and advance rates between 100 and 300 mm·s^{-1}. If we have higher advance rates, the plasma atmospheric effect was not as effective and some adhesion properties were lost.

These results in adhesion improvement matched the results obtained in the quantification of the surface wettability, contact angles, and the increase in the PLA surface free energy for exactly the same plasma conditions: 10 mm and 100–300 mm s^{-1}. For these optimal plasma conditions, the effectiveness of the surface treatment was the highest. Plasma-acting mechanisms such as surface abrasion and insertion of polar groups showed an interesting synergistic effect that leads to a remarkable increase in adhesive properties.

ACKNOWLEDGMENTS

I wish to acknowledge the assistance in the completion of this article the Phd Rafael Antonio Balart Gimeno.

REFERENCES

1. Weber, C. J.; Haugaard, V.; Festersen, R.; Bertelsen, G. *Food Addit. Contam.* **2002**, *19*, 172.
2. Drumright, R. E.; Gruber, P. R.; Henton, D. E. *Adv. Mater.* **2000**, *12*, 1841.
3. Madhavan Nampoothiri, K.; Nair, N. R.; John, R. P. *Bioresour. Technol.* **2010**, *101*, 8493.
4. Arora, A.; Padua, G. W. *J. Food Sci.* **2010**, *75*, R43.
5. Del Nobile, M. A.; Conte, A.; Buonocore, G. G.; Incoronato, A. L.; Massaro, A.; Panza, O. *J. Food Eng.* **2009**, *93*, 1.
6. Harris, A. M.; Lee, E. C. *J. Appl. Polym. Sci.* **2010**, *115*, 1380.
7. John, M. J.; Anandjiwala, R. D.; Pothan, L. A.; Thomas, S. *Compos. Interfaces* **2007**, *14*, 733.
8. Caro, J. C.; Lappan, U.; Simon, F.; Pleul, D.; Lunkwitz, K. *Eur. Polym. J.* **1999**, *35*, 1149.
9. Ferrero, F.; Bongiovanni, R. *Surf. Coat. Technol.* **2006**, *200*, 4770.
10. Foldes, E.; Toth, A.; Kalman, E.; Fekete, E.; Tomasovszky-Bobak, A. *J. Appl. Polym. Sci.* **2000**, *76*, 1529.
11. Jorda-Vilaplana, A.; Fombuena, V.; Garcia-Garcia, D.; Samper, M. D.; Sanchez-Nacher, L. *Eur. Polym. J.* **2014**, *58*, 23.
12. 정진석, 류욱연, Suk, C. H. *Korean Chem. Eng. Res.* **2009**, *47*, 59.
13. Marcinauskas, L.; Grigonis, A.; Valatkevicius, P. *J. Optoelect. Adv. Mater.* **2010**, *12*, 829.
14. Mittal, K. L. *VSP/Brill* **2004**, *4*.
15. Mittal, K. L. Polymer Surface MOdification: Relevance to Adhesion, **2007**.
16. Du, Y.; Yan, N.; Kortschot, M. T. *J. Mater. Sci.* Springer Science+Business Media, New York. **2014**, *49*, 2018.
17. Slepicka, P.; Michaljanicova, I.; Kasalkova, N. S.; Kolska, Z.; Rimpelova, S.; Ruml, T.; Svorcik, V. *J. Mater. Sci.* **2013**, *48*, 5871.
18. Hossain, K. M. Z.; Ahmed, I.; Parsons, A. J.; Scotchford, C. A.; Walker, G. S.; Thielemans, W.; Rudd, C. D. *J. Mater. Sci.* **2012**, *47*, 2675.
19. Ou, R.; Xie, Y.; Shen, X.; Yuan, F.; Wang, H.; Wang, Q. *J. Mater. Sci.* **2012**, *47*, 5978.
20. Bertomeu, D.; Garcia-Sanoguera, D.; Fenollar, O.; Boronat, T.; Balart, R. *Polym. Compos.* **2012**, *33*, 683.

21. Vergne, C.; Buchheit, O.; Eddoumy, F.; Sorrenti, E.; Di Martino, J.; Ruch, D. *J. Eng. Mater. Technol. Trans. ASME* **2011**, *133*, 030903.

22. Encinas, N.; Diaz-Benito, B.; Abenojar, J.; Martinez, M. A. *Surf. Coat. Technol.* **2010**, *205*, 396.

23. Fowkes, F. M. **1968**, 60, 8.

24. Michalski, M. C.; Hardy, J.; Saramago, B. J. V. *J. Colloid Interface Sci.* **1998**, *208*, 319.

25. Owens, D. K. a. R. C. W. *J. Appl. Polym. Sci.* **1969**. *13*, 1741.

26. Shenton, M. J.; Stevens, G. C. *J. Phys. D-Appl. Phys.* **2001**, *34*, 2761.

27. Zenkiewicz, M. *Polimery* **2006**, *51*, 584.

28. Kavc, T.; Kern, W.; Ebel, M. F.; Svagera, R.; Polt, P. *Chem. Mat.* **2000**, *12*, 1053.

29. Borris, J.; Dohse, A.; Hinze, A.; Thomas, M.; Klages, C.-P.; Moebius, A.; Elbick, D.; Weidlich, E.-R. *Plasma Process. Polym.* **2009**, *6*, S258.

30. Cheng, C.; Zhang, L. Y.; Zhan, R. J. *Surf. Coat. Technol.* **2006**, *200*, 6659.

31. De Geyter, N.; Morent, R.; Leys, C. *IEEE Trans. Plasma Sci.* **2008**, *36*, 1308.

32. De Geyter, N.; Morent, R.; Leys, C.; Gengembre, L.; Payen, E.; Van Vlierberghe, S.; Schacht, E. *Surf. Coat. Technol.* **2008**, *202*, 3000.

33. Hwang, Y. J.; Matthews, S.; McCord, M.; Bourham, M. *J. Electrochem. Soc.* **2004**, *151*, C495.

34. Hwang, Y. J.; Qiu, Y.; Zhang, C.; Jarrard, B.; Stedeford, R.; Tsai, J.; Park, Y. C.; McCord, M. *J. Adhes. Sci. Technol.* **2003**, *17*, 847.

35. Teraoka, F.; Nakagawa, M.; Hara, M. *Dent. Mater. J.* **2006**, *25*, 560.

36. Thurston, R. M.; Clay, J. D.; Schulte, M. D. *J. Plast. Film Sheeting* **2007**, *23*, 63.

37. Balart, J.; Fombuena, V.; Espana, J. M.; Sanchez-Nacher, L.; Balart, R. *Mater. Des.* **2012**, *33*, 1.